CDF/PUB/MIN_BIAS/CDFR/6075

K_s^0 and Λ^0 Production Studies in $p\bar{p}$ Collisions at $\sqrt{\text{s}} = 1800$ and 630 GeV

M.Deninno, N.Moggi, F.Rimondi

Version 1.0

Abstract

We present a study of the production of K_s^0 and Λ^0 in minimum bias interactions at $\sqrt{s}$= 1800 and 630 GeV. Comparative analyses of various inclusive distributions and correlations for soft and hard sub-samples of the minimum bias data at the two energies are described.

1 INTRODUCTION

Besides the lighter quarks u and d, strangeness production is the only component of low p_T multiparticle interactions to be statistically significant and experimentally accessible with a Minimum-Bias (MB) trigger. It is also a valid probe to investigate the transition of soft hadron interactions to the high p_T QCD perturbative region.

This paper describes an analysis of K_s^0 and Λ^0 production in $p\bar{p}$ interactions and is part of a low p_T multiparticle production systematic study structured in comparative analyses of statistical distributions and particle correlations at different c.m.s. energies (E_{cms}). Specific emphasis is given to the dependence of the particle correlations on charged multiplicity and to the "hardness" of the interaction.

Inclusive distributions of the multiplicity and transverse momentum of K_s^0 and Λ^0 are presented first. The high statistics of the data sample collected at $\sqrt{s}$= 1800 and 630 GeV allows to extend the range of these measurements and their precision with respect to previous ones.

Studies of the dependence of the average p_T of $K_s^0(\Lambda^0)$ and of their mean number on the event charged multiplicity are also presented.

In analogy with a previous paper [1], which concerns charged particle production, the whole analysis was repeated on two different types of events that have been selected by dividing MB data into soft and hard sub-samples. A different behavior of these sub-samples, already reported for charged particles, is observed once again.

2 DATA SET AND EVENT SELECTION

Data samples have been collected with the CDF detector at the Fermilab Tevatron Collider. The CDF apparatus has been described elsewhere [2]; here only the parts of the detector utilized for the present analysis are discussed. Data at 1800 GeV were collected with a minimum bias trigger during Run 1A and 1B, and at 1800 and 630 GeV during Run 1C. This trigger requires coincident hits in scintillator counters located at 5.8 m on either side of the nominal interaction point and covering the pseudo-rapidity ($\eta = -\log(\tan(\theta/2))$ where θ = angle with respect to the proton direction) interval $3.2 < |\eta| < 5.9$, in coincidence with a beam-crossing signal.

The analysis uses charged tracks reconstructed within the Central Tracking Chamber (CTC). The CTC is a cylindrical drift chamber covering a η interval of about three units with full efficiency for $|\eta| \leq 1$ and $p_T \geq 0.4$ GeV/c.

The inner radius of the CTC is 31.0 cm and the outer radius is 132.5 cm. The full CTC volume is contained in the superconducting solenoidal magnet which operates at 1.4 T [3]. The CTC has 84 sampling wire layers, organized in 5 axial and 4 stereo "superlayers" [4]. Axial superlayers have 12 radially separated layers of sense wires, parallel to the z-axis (the beam axis), that measure the r-ϕ position of a track. Stereo superlayers have 6 sense wire layers, with a $\sim 3°$ stereo angle, that measure a combination of r-ϕ and z information. The stereo angle direction alternates at each stereo superlayer. Axial and stereo data are combined to form a three-dimensional track.

The spatial resolution of each point measurement in the CTC is less than 200 μm; the transverse momentum resolution, including multiple scattering effects, is $\sigma_{p_T}/p_T^2 \leq 0.003$ (GeV/c).

Inside the CTC inner radius, a set of time projection chambers (VTX) [5] provides r-z tracking information out to a radius of 22 cm for $|\eta| < 3.25$. The VTX is used in this analysis to find the z position of event vertices, defined as a set of tracks converging to the same point along the z-axis. Reconstructed vertices are classified as either "primary" or "secondary" based upon several parameters: the number of converging track segments (with a minimum of four within $|\eta| < 3$), the total number of hits used to form a segment, forward-backward symmetry and vertex isolation. Isolated, higher multiplicity vertices with highly symmetric topologies are typically classified as primary; lower mulitiplicity, highly asymmetric vertices or those with few hits in the reconstructed tracks are typically classified as secondary. Systematic uncertainties introduced by the vertex classification scheme are discussed in Section 7.

The transverse energy flux was measured by a calorimeter system [6] covering from -4.2 to 4.2 in η. The system [6] consists of three sub-systems, each with separate electromagnetic and hadronic compartments: the central calorimeter, covering the range $|\eta| < 1$; the end-plug, covering $1 < |\eta| < 2.4$; and the forward calorimeter, covering $2.2 < |\eta| < 4.2$. Energy measurements are made within projective "towers" that span 0.1 units of η and 15° in aximuth (ϕ) within the central calorimeter, and 5° in the end-plug and forward calorimeters.

The 1800 GeV data sample consists of sub-samples collected during three different time periods. Approximately 1,700,000 events were collected in run 1A at an average luminosity of 3.3×10^{30} s^{-1}cm^{-2}, 1,500,000 in run 1B at an average luminosity of 9.1×10^{30} s^{-1}cm^{-2} and 106,000 in run 1C at an average luminosity of 9.0×10^{30} s^{-1}cm^{-2}. The 630 GeV data set consists of about 2,600,000 events recorded during run 1C at an average luminosity of 1.3×10^{30} s^{-1}cm^{-2}.

Additional event selection conducted offline removed the following events: (i) events identified as containing cosmic-ray particles as determined by time-of-flight measurements using scintillator counters in the central calorimeter; (ii) events with no reconstructed tracks; (iii) events exhibiting symptoms of known calorimeter problems; (iv) events with at least one charged particle reconstructed in the CTC to have $p_T > 400$ MeV/c, but no central calorimeter tower with energy deposition above 100 MeV; (v) events with more than one primary vertex; (vi) events with a primary vertex more than 60 cm away from the center of the detector (in order to keep full tracking efficiency in the CTC and avoid energy leakage through exposed cracks in the calorimeter). (vii) events with no primary vertices.

After all event selection cuts, 2,079,558 events remain in the full minimum bias sample at $\sqrt{s} = 1800$ GeV (runs 1A + 1B + 1C), and 1,963,157 in that at $\sqrt{s} = 630$ GeV (run 1C).

The vast majority of rejected events failed the vertex selection. About 0.01% of selected events contain background tracks from cosmic rays that are coincident in time with the beam crossing and pass near the event vertex. The residual beam gas contamination is about 0.02%.

See ref. [1] for a complete discussion of the systematic uncertainties that arise from the event selection criteria and other sources.

3 TRACK SELECTION

Reconstructed tracks within each event must pass selection criteria designed to remove the main sources of background. Tracks must pass through a minimum number of layers in the CTC, and have a minimum number of hits in each superlayer in order to reduce the number of tracks with reconstruction errors. Fake and secondary particle tracks are removed by requiring that tracks pass within 0.5 cm of the beam axis, and within 5 cm along the z-axis of the primary event vertex. Accepting only tracks with $p_T \geq 0.4$ GeV/c and within $|\eta| \leq 1.0$ ensures full efficiency and acceptance.

We define the charged track multiplicity in an event, $N^{\star}_{ch}$, as the number of selected CTC tracks in the event.

4 K^0_s and Λ^0 SELECTION

K^0_s and Λ^0 (from now on collectively V^0) are selected from the full sample of the CTC reconstructed tracks, looking for unlike charge pairs converging to a common secondary vertex. A 1-constraint fit is performed for the two tracks coming from the secondary vertex with both the hypotheses of K^0_s and Λ^0 decay [1]. A $K^0_s(\Lambda^0)$ candidate is selected if the fit has a probability greater than 5% and the fitted mass is within five standard deviations from the nominal mass. Subsequent analysis cleaning restricts this selection to a fit probability >5% for the 3-C fit and mass determination within three standard deviations.

Our analysis selection also requires that:

- $L_{xy}(V^0) \geq 1.0$ cm, where L_{xy} is the secondary vertex displacement in the $x-y$ plane;
- decayed tracks are within $|\eta| \leq 1.5$ and $p_T \geq 0.3$ GeV/c;
- the V^0 line-of-flight is close to the event vertex along the z axis so that $|Z_0^{V^0} - Z^{vertex}| < 6$ cm;
- impact parameter $d_0(V^0) < 0.7$ cm;
- $p_T(V^0) > 0.4$ GeV/c and $|\eta(V^0)| < 1.0$

In case that more than a V^0 candidate is found in the same event, a further check is done to ensure that the same track is not used in more than one vertex fit. When this happens only the best fit is retained and the other rejected.

After all selection cuts we find in the 1800 GeV MB sample 36,642 K^0_s and 7,518 Λ^0; in the 630 GeV MB sample 32,222 K^0_s and 5,883 Λ^0.

The invariant mass distributions of the K^0_s and Λ^0 surviving the selection cuts are shown in Fig. 1. In both cases the background is negligible.

[1] As we do not distinguish Λ^0 from $\bar{\Lambda}^0$, in this paper Λ^0 stands for both.

5 EFFICIENCY CORRECTIONS

The efficiency for finding $K_s^0(\Lambda^0)$ has been investigated in two different ways. In the first method simulated hits from single generated V^0 are embedded among the set of hits of real MB events. The full real events including the embedded hits are then reconstructed with standard V^0 search and selection. In the second method full MB events with V^0 production and decay are generated with Pythia/Jetset Monte-Carlo [2]. The full event is then simulated through the CDF detector and reconstructed.

The efficiency is computed as the ratio of the reconstructed to the generated number of V^0 in the acceptance region. It is then examined as a function of single kinematical variables of the V^0 itself, independently of all the others, that is integrating over all the the remaining variables.

The efficiency for finding one single K_s^0 is almost constant around 50% (40% for Λ^0) in the phase-space region delimited by $|\eta| <1$ and $p_T \geq 2.0$ GeV/c, and strongly decreasing outside this region down to about 15% (10% for Λ^0). The efficiency also diminishes for $L_{xy} \lesssim 3$ cm, but is roughly constant as a function of the charged multiplicity of the event. A strong reduction is observed when looking to events that contain more than one V^0. The overall efficiency is about 31% for K_s^0 and 27% for Λ^0.

A correction factor for the fiducial acceptance cut in L_{xy} and in the p_T of the V^0 decay products was computed with MC and found to be ranging from $\simeq 10$ at $p_T = 0.4$ GeV/c to about 1.02 for $p_T \gtrsim 5$ GeV/c.

The contamination of Λ^0 in the K_s^0 sample was estimated to be $\simeq 3\%$; viceversa the contamination of K_s^0 in the Λ^0 sample about 7%, with a peak of almost 50% for $p_T <$ 1.5 GeV/c.

The overall final correction takes into account also the probability of selecting secondary vertices which are not due to K_s^0 or Λ^0 decays. This factor accounts for roughly 20% of the K_s^0 and 30% of the Λ^0.

In order to check the $K_s^0(\Lambda^0)$ selection and the quality of the efficiency correction we show in Figs. 2 and 3 the raw and the corrected lifetime distributions at 1800 GeV. A fit to an exponential form gives K_s^0 mean lifetime of $(0.881 \pm 0.006)10^{-10}$ sec for 1800 GeV and $(0.912 \pm 0.007)10^{-10}$ sec for 630 GeV. Both values are quite close to the known values. The same fit to the Λ^0 lifetime distributions gives mean lifetime of $(2.62 \pm 0.08)10^{-10}$ sec for 1800 GeV and $(2.59 \pm 0.08)10^{-10}$ sec for 630 GeV.

Finally, we refer to [1] for a detailed discussion of the charged track selection and reconstruction efficiencies.

[2] Version 5_7 of Pythia together with Jetset 7_4 were used. See ref. [1] for the details of the configuration employed.

6 SELECTION OF *SOFT* AND *HARD* INTERACTIONS

The identification of "soft" and "hard" interactions is largely a matter of definition [7] since it is unknown how to distinguish soft and hard parton interactions at high impact parameter. This is true either from the theoretical and the experimental point of view. In this analysis we use a jet reconstruction algorithm to distinguish between the two classes. The algorithm employs a cone with radius $R = (\Delta\eta^2 + \Delta\phi^2)^{1/2} = 0.7$ to define "clusters" of calorimeter towers belonging to the jet. To be considered, a cluster must have a transverse energy (E_T) of at least 1 GeV in a seed tower, plus at least 0.1 GeV in an adjacent tower.

In the regions $|\eta| < 0.02$ and $1.1 < |\eta| < 1.2$, a track clustering algorithm is used instead of the calorimeter algorithm in order to compensate for energy lost in calorimeter cracks. A track cluster is defined as one track with $p_T > 0.7$ GeV/c and at least one other track with $p_T \geq 0.4$ GeV/c in a cone of radius $R = 0.7$.

We define a *soft* event as one that contains no cluster with $E_T > 1.1$ GeV. All other events are classified as *hard*.

7 SYSTEMATIC UNCERTAINTIES

The main source of systematic errors is the acceptance and efficiency correction procedure. As described in Section 5, acceptance and efficiency corrections have been computed by MC simulation. The shape of the MC generated distributions of V^0 may sensibly affect the results of this computation. Moreover, the efficiency depends also on the reliability of the simulation of the apparatus. Both these effects have been extimated using modified MC generated distributions and applying different simulation procedures (see Section 5). A maximum 14% systematic uncertainty due to this source is attributed to the experimental distributions shown in this paper.

Other possible sources of systematic effects can be the large spread of the instant luminosity during the recording of the full data sample and the uncertainty associated to the identification and selection of good isolated $p\bar{p}$ interactions from secondary and close event vertices (see [1]). The first may affect the results because higher luminosity gives higher detector occupancy which in turn can alter the V^0 identification. It has been investigated analysing data samples recorded with different instant luminosities. The results show no observable effect.

The second source can lead to a wrong event selection and to produce associations of tracks that fake a V^0. This source has been investigated comparing data samples with different good $p\bar{p}$ vertex selections [1]. The results give systematic variations smaller than 9% on the overall number of $K_s^0(\Lambda^0)$.

Combining the contribution from the different sources, it is concluded that a 16% systematic error affects the present results.

8 ANALYSIS RESULTS and DISCUSSIONS

8.1 Results

In Table 1 are shown the raw and corrected numbers of $K_s^0(\Lambda^0)$ selected in our fiducial region for the full MB as well as for the *soft* and the *hard* samples. The corrected mean number of $K_s^0(\Lambda^0)$ per event in each sample is also shown. All data presented in this paper are measured in $p_T \geq 0.4$ GeV/c and $|\eta| \leq 1.0$, as specified in Section 4, and are corrected for acceptance and finding efficiency.

In Fig. 4 for the K_s^0 and in Fig. 5 for the Λ^0, is shown the normalized multiplicity of $K_s^0(\Lambda^0)$ for the MB, *soft* and *hard* events. Results for the $\sqrt{s}$=1800 (full symbols) and 630 GeV (open symbols) data are shown. These distributions represent the probabilities of producing one or more $K_s^0(\Lambda^0)$ per event. The distributions of multiplicities of Λ^0 are lower than the ones of K_s^0 and their slopes are steeper. This behavior is more pronounced in the soft sub-sample.

		RAW			CORRECTED			N.of $K_s^0(\Lambda^0)$/EVENT (%)		
		MB	Soft	Hard	MB	Soft	Hard	MB	Soft	Hard
1800 GeV	K_s^0	36642	6733	29909	101332 ±6380	19664 ±1702	81311 ±4544	4.9±0.3	2.0±0.2	7.3±0.4
	Λ^0	7518	782	6736	46113 ±12612	10170 ±3951	38902 ±9684	2.2±0.6	1.1±0.4	3.5±0.8
630 GeV	K_s^0	32222	9835	22387	94607 ±8390	29920 ±3080	62856 ±4390	4.8±0.4	2.6±0.3	7.7±0.5
	Λ^0	5883	1098	4785	39119 ±11497	12940 ±5056	29239 ±8048	2.0±0.5	1.1±0.4	3.6±0.9

Table 1: Raw and corrected numbers of K_s^0 and Λ^0 found in each data set. In the rightmost three columns the fraction of $K_s^0(\Lambda^0)$ per event is shown.

The invariant $(1/p_T)dN/d\eta dp_T$ inclusive distributions of kaons are shown in Figs. 6 and 7 at the two energies for the full MB, soft and hard samples. Data are normalized to the number of events in each sample. Figs. 8 and 9 show the same p_T distributions for the Λ^0.

The dependence of the K_s^0 and Λ^0 average p_T on the event charged multiplicity is shown in Figs. 10 to 12 (1800 GeV) and 13 to 15 (630 GeV). The mean p_T of primary charged tracks, measured in the same phase space region, as published in [1], is also shown for comparison.

Figs. 16 to 19 show the ratio of the mean number of $K_s^0(\Lambda^0)$ per event to the multiplicity as a function of the multiplicity itself.

The multiplicity $N_{ch}^{\star}$ was choosen as the reference variable to analyze V^0 production. The reason for this choice is based on the observation that the event charged multiplicity is a global event variable characterizing the whole multiparticle final state and is related to the hardness of the interaction (see [1], [8], [9]). As well as for charged particles, it can be expected that the V^0 final state correlations exhibit possible new structures as a function of $N_{ch}^{\star}$. The dependence of the average p_T on multiplicity, e.g., remains unexplained in any of the current models.

8.2 Analysis Discussion

Some simple observations may be done about the data in Table 1. The percentage of K_s^0 which are produced in the soft sub-sample is rather small, ranging from about 32% at 630 GeV to about 20% at 1800 GeV (respectively 33% and 22% for Λ^0). The corrected mean number of K_s^0 produced per event in the full MB sample is about (4.8±0.4)% at 630 GeV and (4.9±0.3)% at 1800 GeV (respectively (2.0±0.6)% and (2.2±0.6)% for Λ^0).

The K_s^0/π cross section ratio may be obtained by fitting the K_s^0 and charged track invariant p_T distributions in the available p_T range and extrapolating the fitted functions down to p_T=0 (details of the fits are described below). With this technique a ratio of 0.11±0.02 (including the systematic uncertainty) at $\sqrt{s}$=1800 GeV and 0.15±0.03 at 630 GeV is obtained. These measures are in good agreement with previous CDF results ([12]).

	MB	Soft	Hard
1800	0.11±0.02	0.32±0.05	0.09±0.04
630	0.15±0.03	0.31±0.04	0.10±0.06

Table 2: K_s^0/π ratio in each data set. Data are corrected for efficiency and computed in the full p_T assuming that the power-law form of p_T distribution is correct down to p_T=0 GeV/c.

In Table 2 the corresponding values for the soft and hard sub-samples are reported: it is remarkable that this ratio is at least two times larger in soft than in MB events.

Studies of the production of strange particles K_s^0 and Λ^0 in proton-antiproton interactions at different $\sqrt{s}$ are described in ref. [10] at $\sqrt{s}$=540 GeV and [11] at 200 and 900 GeV. In ref. [12]-[14] results at $\sqrt{s}$=1800 GeV are presented. Comparison with our results is of course restricted to the full MB samples; furthermore it should not be ignored that here no absolute cross-sections are provided. Comparison with ref. [10], [11] and [13] also requires taking into account the different p_T and η selected regions.

A direct comparison of the invariant p_T distribution of K_s^0 can be done with ref. [12]. Other measures have been done at different energies and in different phase space regions (refs. [10]-[11], [13]-[14]).

In ref. [12] the p_T distribution of K_s^0 was fitted to the functional power-law form:

$$E\frac{d^3N_k}{dp^3} = A\left(\frac{p_0}{p_0 + p_T}\right)^n \tag{1}$$

fixing the parameter p_0 to 1.3 GeV/c. Form 1 with the parameters obtained there does not fit our data. The best fit to our distribution was obtained with this form when all the three parameters were let vary freely and restricting the fit region to $p_T >$1.1 GeV/c. Attempts under different conditions were made: a summary of the results is reported in Tables 3.

From our best fit of MB at 1800 GeV the mean p_T is 0.74 ± 0.07 GeV/c (0.70 ± 0.08 GeV/c at 630 GeV). These values are significantly higher than the previous CDF measures.

Taking care of the different conditions and method of measure, it is possible to compare also to UA5 data (ref. [10], [11]): our present result is higher also in this case.

For completeness the fit results of the p_T invariant distribution for the soft sub-sample are also reported. A second fitting function was also used in the form:

$$E\frac{d^3N_k}{dp^3} = exp(A + Bp_T) \tag{2}$$

At both energies we obtain a good χ^2 (see Table 3). The shape of the distribution is therefore well described also by an exponential function; the mean p_T is generally larger than what is yelded by form 1.

For Λ^0 too, a mean p_T systematically higher than other experiments at equivalent energy is obtained (compare with [11] and [13]). In this case the MB data can be equally well fitted by form 1 and an exponential function. A summary of these results is in Table 4.

The mean p_T of V^0 as a function of $N_{ch}^\star$ has been computed as the average p_T of all $K_s^0(\Lambda^0)$ observed in events of given charged multiplicity in our acceptance region ($p_T >$ 0.4 GeV/c).

As can be expected, the increase rate of the K_s^0 mean p_T is always stronger than that of charged tracks. Yet the increase rate of Λ^0 is even stronger, leading to the conclusion that it depends on the particle mass.

Experiment ($\sqrt{s}$ in GeV)	Data Set	$\langle p_T \rangle$ (GeV/c)	p^0 (GeV/c)	n or B	$\chi^2/d.o.f.$	function
UA5 (546)	MB	0.58±0.04	–	–	1.15	P.L.,Exp. (*)
CDF-0 (630)	MB	0.5±0.1	1.3	8.2±1.1	0.37	P.L.
CDF-I (630)	MB	0.70±0.08	3.5±0.3	13.0±0.7	1.4	P.L.
UA5 (900)	MB	0.63±0.03	–	–	0.5	P.L.,Exp. (*)
CDF-0 (1800)	MB	0.60±0.03	1.3	7.7±0.2	0.74	P.L.
CDF-I (1800)	MB	0.61±0.02	1.3	7.26±0.02	7.2	P.L.
CDF-I (1800)	MB	0.74±0.07	3.16±0.06	11.5±0.1	1.1	P.L.
CDF-I (630)	Soft	0.59±0.04	9.4±0.02	34.7±0.2	0.86	P.L.
CDF-I (630)	Soft	0.65±0.04	–	-3.09±0.04	0.95	Exp.
CDF-I (1800)	Soft	0.61±0.02	9.4±0.1	33.4±0.1	0.97	P.L.
CDF-I (1800)	Soft	0.67±0.02	–	-2.98±0.04	1.1	Exp.
(*) UA5 fits to a power-law form in p_T >0.4 together with an exponential form in p_T <0.4 GeV/c						

Table 3: Results of the fit to the invariant p_T distribution of K_s^0. Data at different E_{cms} are reported (for different experiments the parameters of the fit were reported when available). The function used for the fit is shown in the last column: *P.L.* stands for "power-law" (form 1) and "Exp." for "exponential" (form 2); parameters p^0 and n refer to the power-law, A and B to the exponential form. CDF-0 refers to the so called Run-0 of the Tevatron (see [12]) and CDF-I to Run I data (this analysis).

Experiment ($\sqrt{s}$ in GeV)	Data Set	$\langle p_T \rangle$ (GeV/c)	p^0 (GeV/c)	n or B	$\chi^2/d.o.f.$	function
UA5 (546)	MB	0.62±0.08	–	–	–	Exp.
CDF-I (630)	MB	0.90±0.07	12.4±0.8	30.6±0.1	1.0	P.L.
CDF-I (630)	MB	0.97±0.01	–	2.07±0.02	0.67	Exp.
UA5 (900)	MB	0.97±0.01	–	–	–	Exp.
CDF-I (1800)	MB	0.95±0.09	11.2±0.6	27±1	0.76	P.L.
CDF-I (1800)	MB	1.03±0.01	–	-1.94±0.02	0.99	Exp.
CDF-I (630)	Soft	0.66±0.05	10.2±0.5	33.8±0.1	1.0	P.L.
CDF-I (630)	Soft	0.72±0.07	–	-2.76±0.07	1.0	Exp.
CDF-I (1800)	Soft	0.67±0.09	8.9±0.8	30±2	0.60	P.L.
CDF-I (1800)	Soft	0.73±0.10	–	-2.7±0.1	0.60	Exp.

Table 4: Results of the fit to the invariant p_T distribution of Λ^0. Data at different E_{cms} are reported (for different experiments the parameters of the fit were reported when available). The function used for the fit is shown in the last column: *P.L.* stands for "power-law" (form 1) and "Exp." for "exponential" (form 2); parameters p^0 and n refer to the power-law, A and B to the exponential form. CDF-I refers to Run I data (this analisis).

The same kind of analysis is reported also in ref. [14]. A direct comparison is not possible because of the different p_T range considered and η acceptance, which reflects in larger multiplicities. A slope raise with heavier particle masses is clearly observable.

In the analysis of charged tracks [1] it was emphasized a different behavior with respect to E_{cms} of the correlation in MB and in the hard samples, while a clear invariance was seen in the soft sample. With the available $K_s^0(\Lambda^0)$ statistics it is not possible to enphasize any difference of the $\langle p_T \rangle$ dependence with multiplicity at the two energies, even in the full MB sample. This is even more so for the soft and hard sub-samples. Nevertheless the behavior of the three sub-samples is clearly different.

It is worth to mention that the mean $K_s^0(\Lambda^0)$ p_T increases with $N_{ch}^\star$ also in the soft sub-sample, a feature which is not explained by the current models([1],[8],[9],[15],[16]). This observation holds also for charged hadrons, as was discussed in [1].

The ratios of the mean numbers of $K_s^0(\Lambda^0)$ per event to the charged multiplicity drop in the first few bins and are roughly constant for $N_{ch}^\star \geq 6$ (MB sample) for both K_s^0 and Λ^0. The dependence on $N_{ch}^\star$ is more pronounced for K_s^0 than for Λ^0. The fraction of Λ^0 per event and per track is obviously smaller than that of K_s^0 and for both is larger at 630 GeV than at 1800 GeV.

Finally, it should be mentioned that the soft Λ^0 sample is not sensibly different from the full MB. This is not true for K_s^0, where the difference is visible at both energies.

9 CONCLUSIONS

The present measures extend to K_s^0 and Λ^0 production the studies of the charged particle properties in minimum-bias $p\bar{p}$ interactions.

High statistics and high precision measurement of track momentum, together with accurate efficiency corrections, give substantial improvement to the existing data.

The data available at the two c.m.s. energies, with similar statistics, allow direct comparison of measures obtained in the same experimental conditions.

- The overall production rates of K_s^0 and Λ^0 are in agreement with previous measurements.
- The inclusive p_T spectra of K_s^0 and Λ^0 extend now to $p_T \geq 8$ GeV/c. The K_s^0 distribution, compared to previous data, shows a different shape. For both K_s^0 and Λ^0, we measure an average p_T significantly higher.
- New results are presented on the distribution of multiplicity of K_s^0 and Λ^0.
- For the first time the MB sample has been analysed in its soft and hard sub-components. Inclusive p_T and multiplicity distributions of V^0 are shown also for the soft and hard data.
- Analyses of the correlation of the mean $K_s^0(\Lambda^0)$ p_T on the charged event multiplicity are presented. Comparison with an analogous study performed on charged tracks

indicates that the rate of the dependence grows with particle mass. An increase of the mean p_T is observable also in the soft sub-sample alone.

- The event charged multiplicity has been adopted as the independent variable also to analyse the ratio of the mean number of $K_s^0(\Lambda^0)$ per event to the number of primary charged particles. For both K_s^0 and Λ^0 this ratio drops at very low multiplicity, keeping roughly constant for $N_{ch}^{\star} \gtrsim 5$.

References

[1] D. Acosta *et al.*, Phys. Rev. D**65**, 072005 (2002);

[2] F. Abe *et al.*, Nucl. Instrum. Methods A**271**, 387 (1988), and references therein.

[3] F. Abe *et al.*, Phys. Rev. D**52**, 4784 (1995).

[4] F. Bedeschi *et al.*, Nucl. Instrum. Methods A**268**, 50 (1988).

[5] F. Snider *et al.*, Nucl. Instrum. Methods A**268**, 75 (1988).

[6] F. Balka *et al.*, Nucl. Instrum. Methods A**267**, 272 (1988); S. R. Hahn *et al., ibid.* **267**, 351 (1988); K. Yasuoka *et al., ibid.* **267**, 315 (1988); R. G. Wagner *et al., ibid.* **267**, 330 (1988); T. Devlin *et al., ibid.* **267**, 24 (1988); S. Bertolucci *et al., ibid.* **267**, 301 (1988); Y. Fukui *et al., ibid.* **267**, 280 (1988); S. Cihangir *et al., ibid.* **267**, 249 (1988); G. Brandenburg *et al., ibid.* **267**, 257 (1988).

[7] F. Abe *et al.*, Phys. Rev. D**56**, 3811 (1997); Phys. Rev. Lett. **79**, 584 (1997);
X. Wang, Phys. Rev. D**46**, 1900 (1992);
UA1 Collaboration, C. Albajar *et al*, Nucl. Phys. B**309**, 405 (1988).

[8] L. Van Hove, Phys. Lett. B**127**, 138 (1982); R. Hagedorn, Rev. Nuovo Cimento **6**, 10 (1983); J.D. Bjorken, Phys. Rev. D**27**, 140 (1983).

[9] X. Wang and C. Hwa, Phys. Rev. D**39**, 187 (1989); M. Jacob, CERN preprint CERN/TH. 3515 (1983); F.W. Bopp, P. Aurenche, and J. Ranft, Phys. Rev. D**33**, 1867 (1986).

[10] K.Alpgard *et al.*, UA5 Collaboration, Phys. Lett. B**115**, 315 (1982); G.J.Alner *et al.*, UA5 Collaboration, Nucl. Phys. B**258**,505 (1985);

[11] R.E.Ansorge *et al.*, UA5 Collaboration, Phys. Lett. B**199**, 311 (1987);

[12] F.Abe *et al.*, CDF Collaboration, Phys. Rev. D**40**, 3791 (1989);

[13] S.Banerjee *et al.*, E735 Collaboration, Phys. Rev. Lett. **62**, 12 (1989;

[14] T.Alexopoulus, II Int.Conf. on Phys. and Astrophys. of Quark-Gluon Plasma, Calcutta, January 1993.

[15] T. Sjöstrand and M. van Zijl, Phys. Rev. D**36**, 2019 (1987), and references therein.

[16] S. Barshay, Phys.Lett. B**127**, 129 (1983).

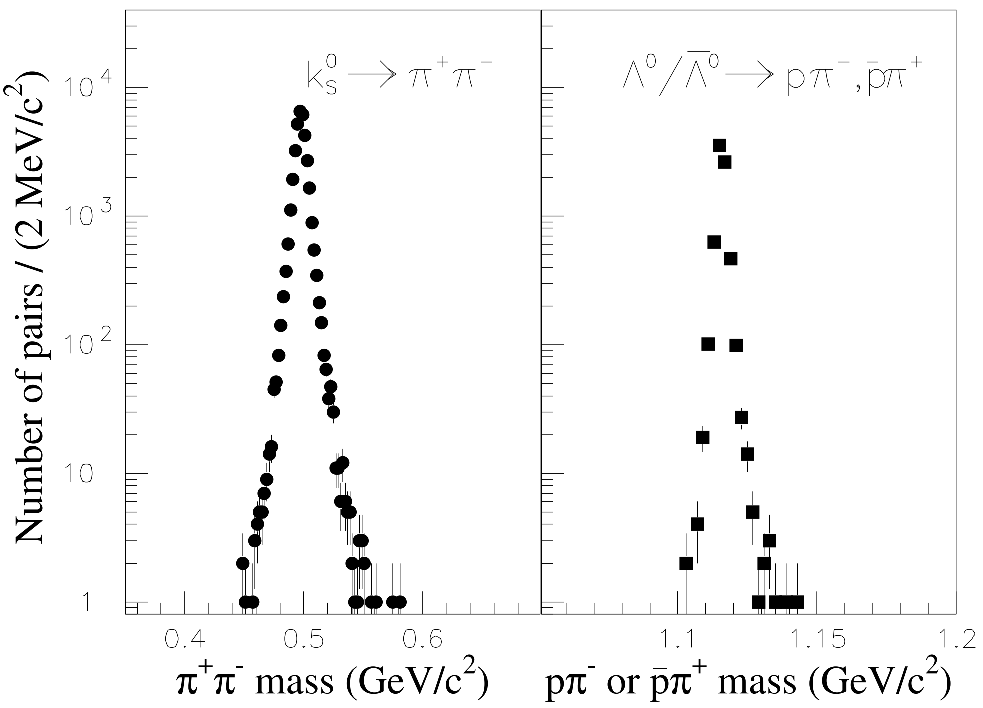

Figure 1: Invariant mass with a $\pi - \pi$ and π-p mass assignement for oppositely signed track pairs passing all selection cuts. 1800 GeV data are shown.

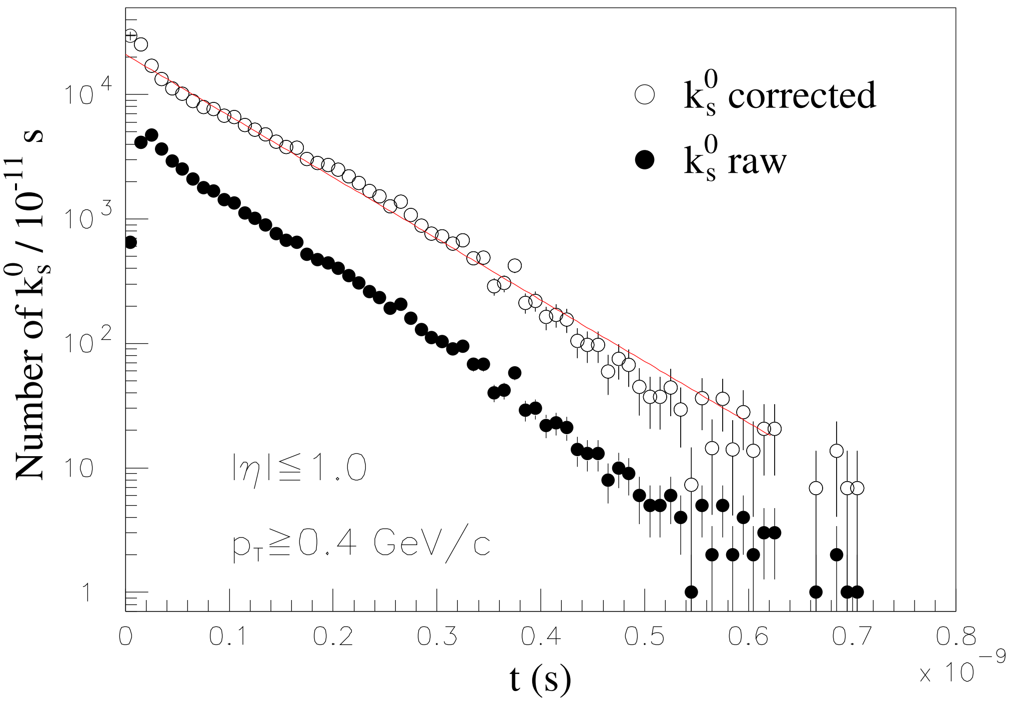

Figure 2: Raw and corrected K_s^0 lifetime distribution for 1800 GeV data.

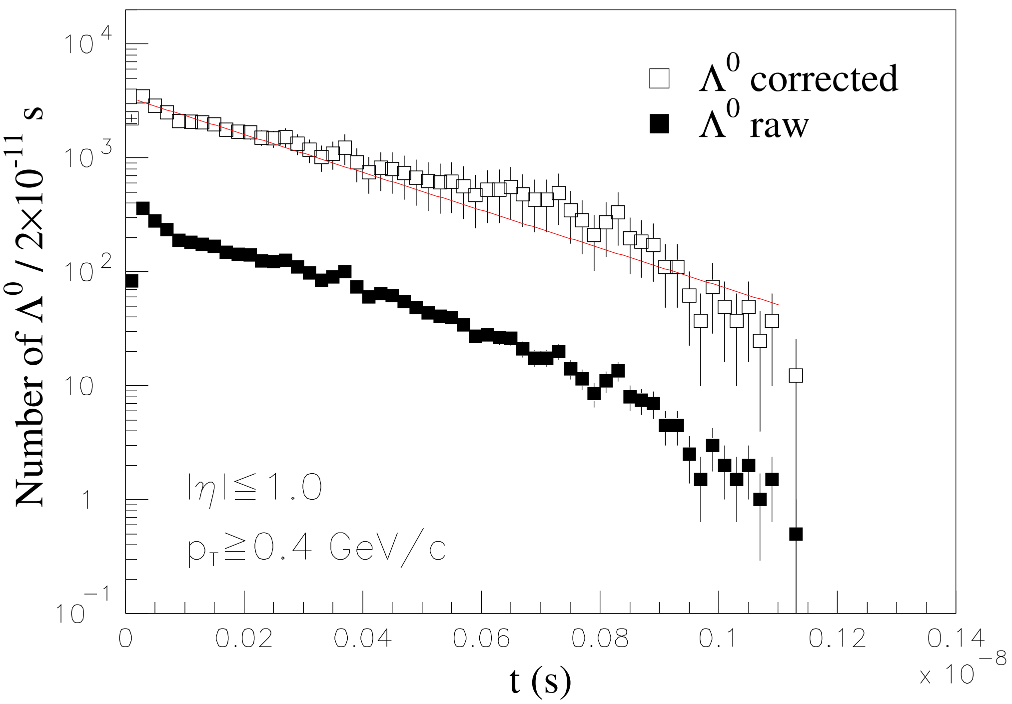

Figure 3: Raw and corrected Λ^0 lifetime distribution for 1800 GeV data.

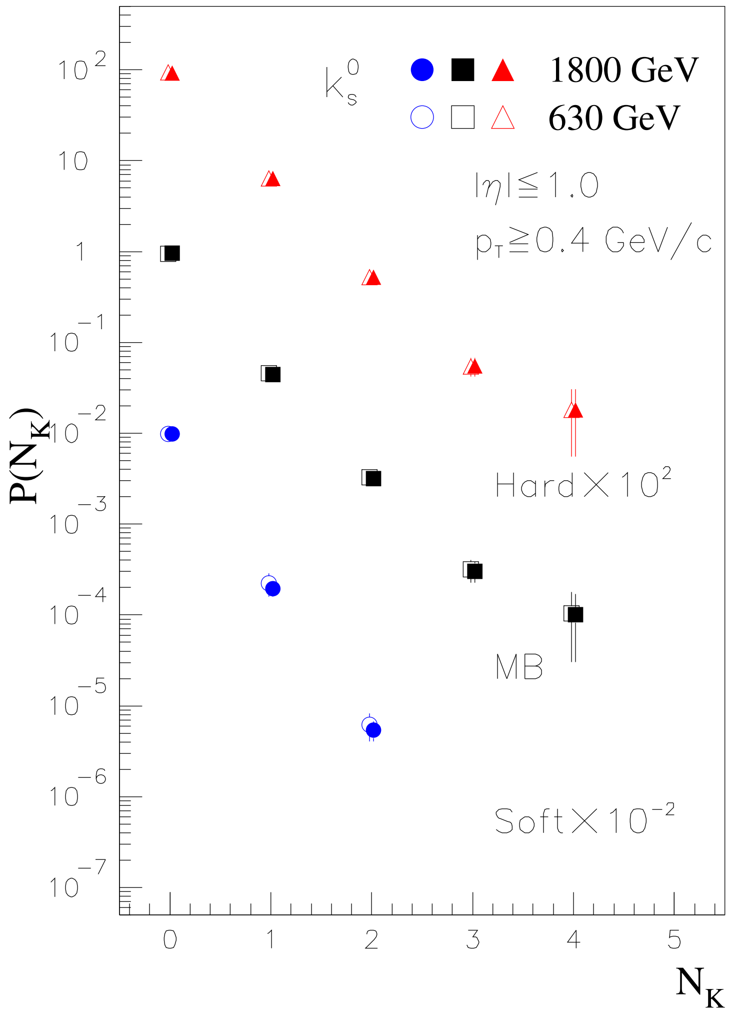

Figure 4: Distribution of the multiplicity of K_s^0 at 1800 (full symbols) and 630 GeV (open symbols). MB, soft (divided by 100) and hard data (multiplied by 100) are shown.

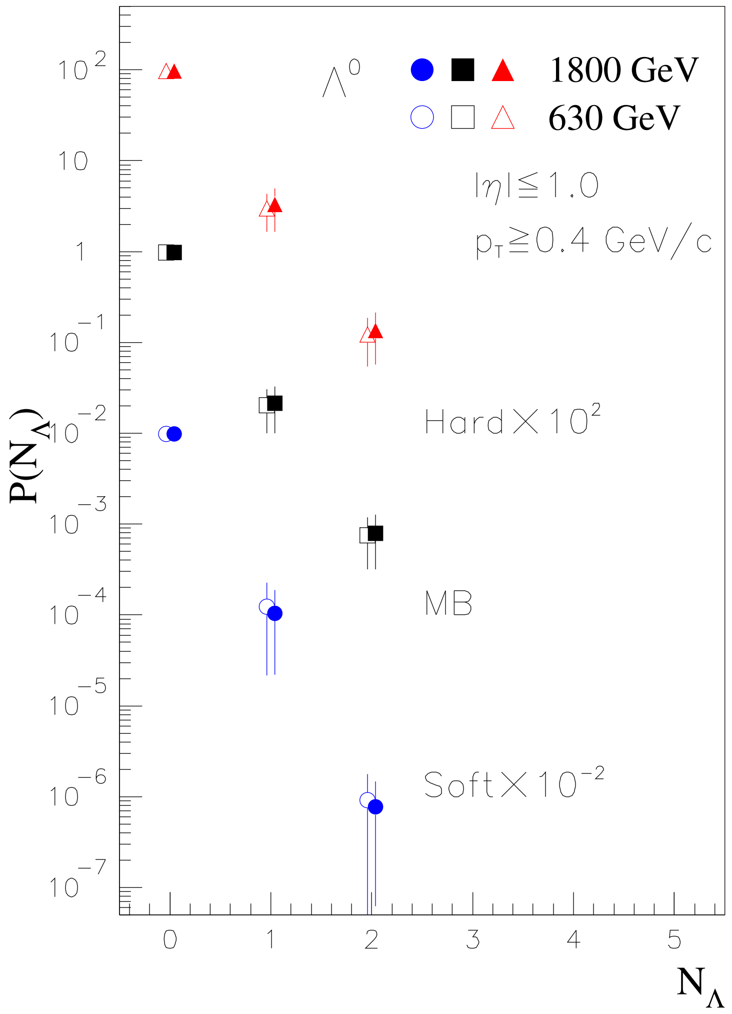

Figure 5: Distribution of the multiplicity of Λ^0 at 1800 (full symbols) and 630 GeV (open symbols). MB, soft (divided by 100) and hard data (multiplied by 100) are shown.

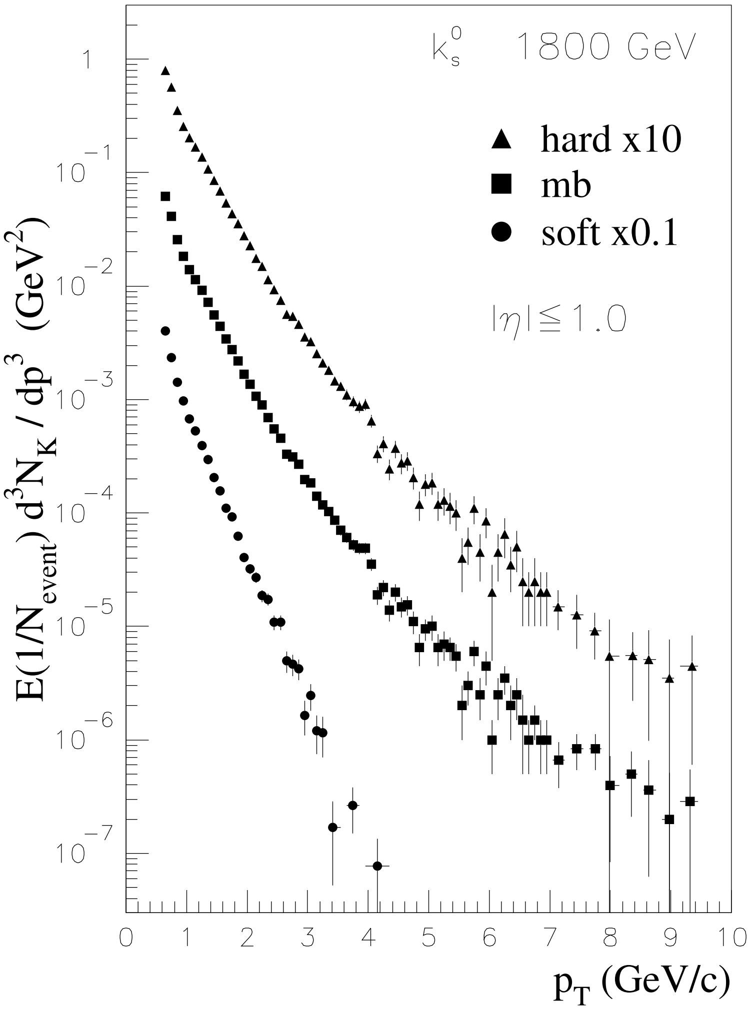

Figure 6: K_s^0 inclusive invariant p_T distributions at 1800 GeV. MB, soft and hard data are shown, each normalized to its number of events. For clearness hard data points are multiplied by 10 and soft data points by 0.1.

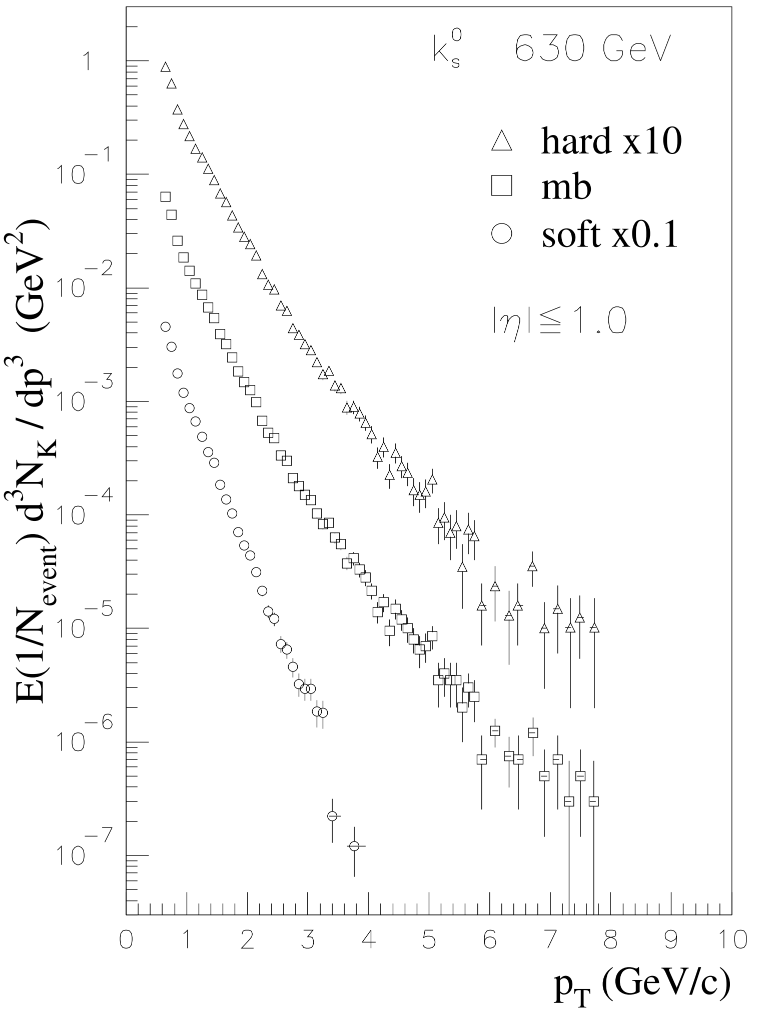

Figure 7: K_s^0 inclusive invariant p_T distributions at 630 GeV. MB, soft and hard data are shown, each normalized to its number of events. For clearness hard data points are multiplied by 10 and soft data points by 0.1.

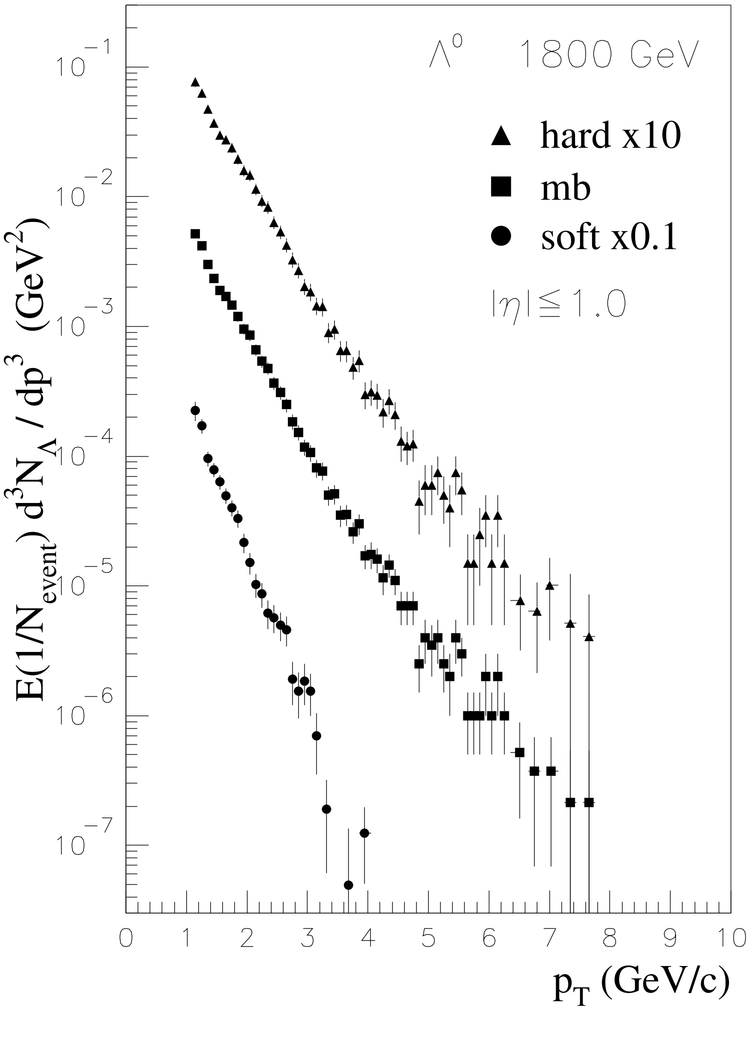

Figure 8: Λ^0 inclusive invariant p_T distributions at 1800 GeV. MB, soft and hard data are shown, each normalized to its number of events. For clearness hard data points are multiplied by 10 and soft data points by 0.1.

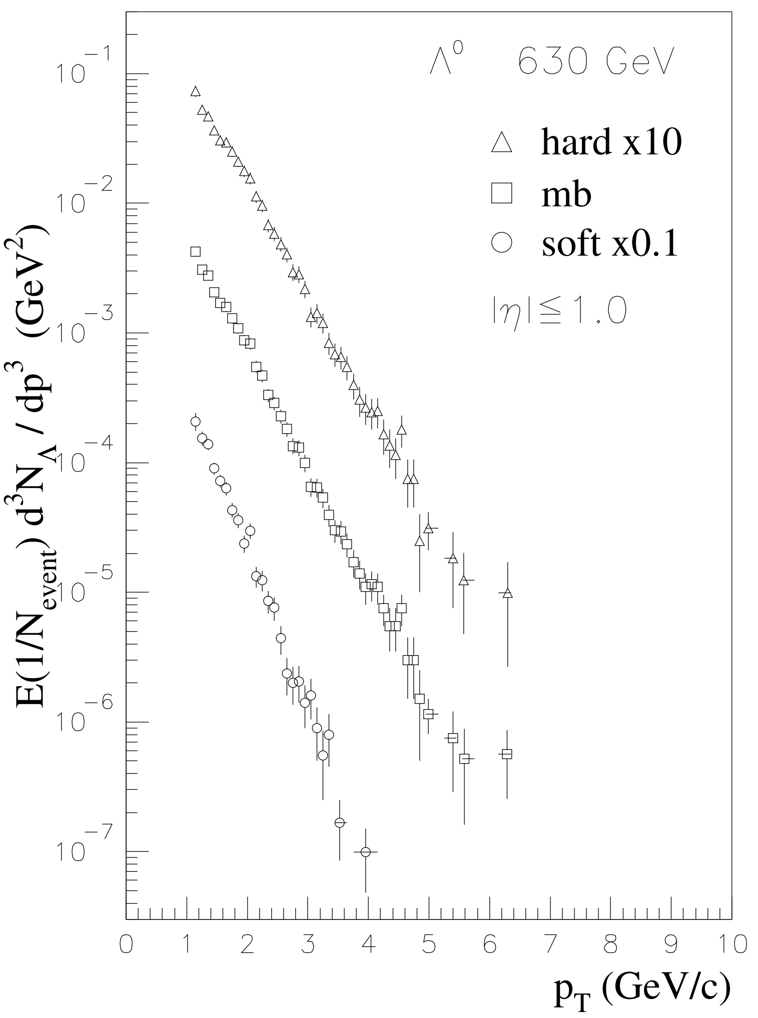

–

Figure 9: Λ^0 inclusive invariant p_T distributions at 630 GeV. MB, soft and hard data are shown, each normalized to its number of events. For clearness hard data points are multiplied by 10 and soft data points by 0.1.

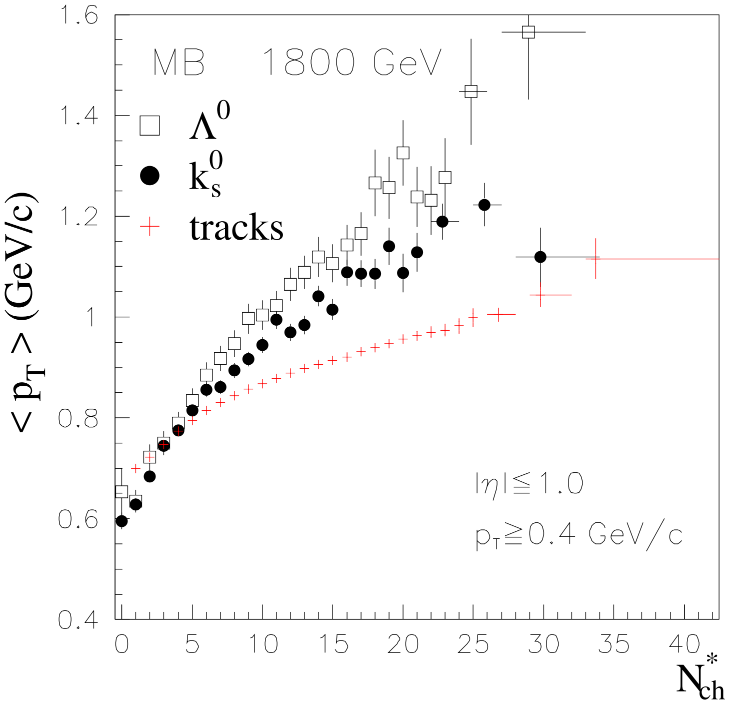

Figure 10: Average transverse momentum $\langle p_T \rangle$ of K_s^0 and Λ^0 at 1800 GeV as a function of the event charged multiplicity ($N^{\star}_{ch}$). MB data are shown. For comparison, also the mean p_T of charged tracks, measured in the same phase space region, is plotted.

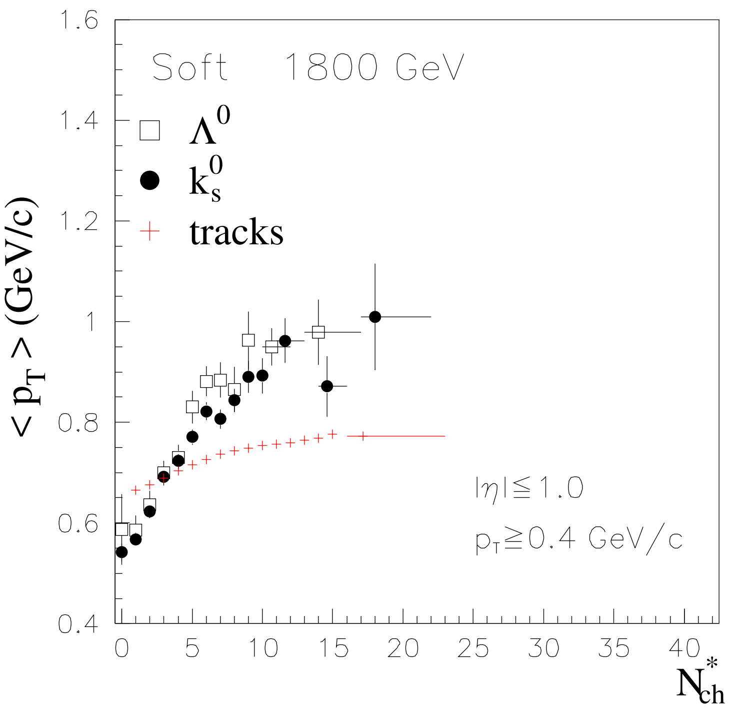

Figure 11: Average transverse momentum $\langle p_T \rangle$ of K_s^0 and Λ^0 at 1800 GeV as a function of the event charged multiplicity ($N_{ch}^{\star}$). Soft data are shown. For comparison, also the mean p_T of charged tracks, measured in the same phase space region, is plotted.

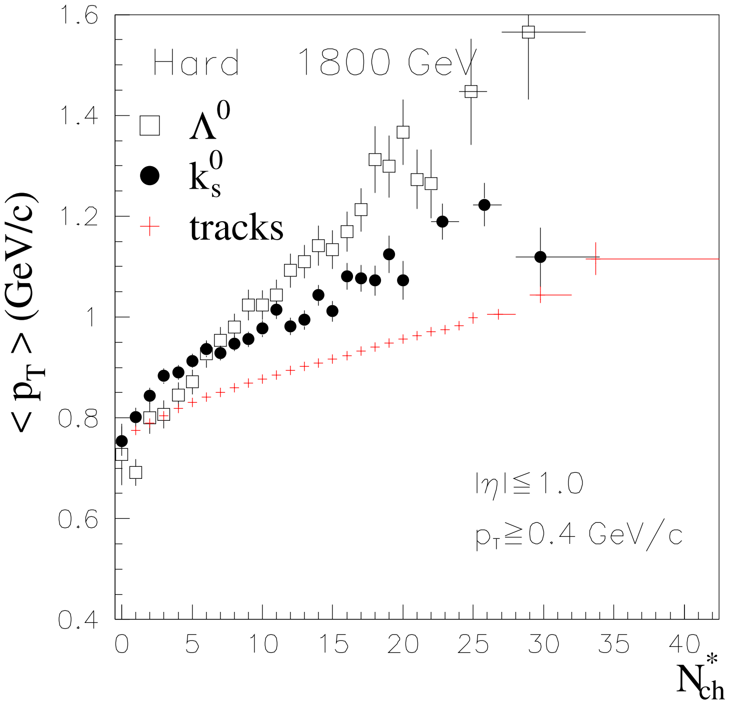

Figure 12: Average transverse momentum $\langle p_T \rangle$ of K_s^0 and Λ^0 at 1800 GeV as a function of the event charged multiplicity ($N_{ch}^{\star}$). Hard data are shown. For comparison, also the mean p_T of charged tracks, measured in the same phase space region, is plotted.

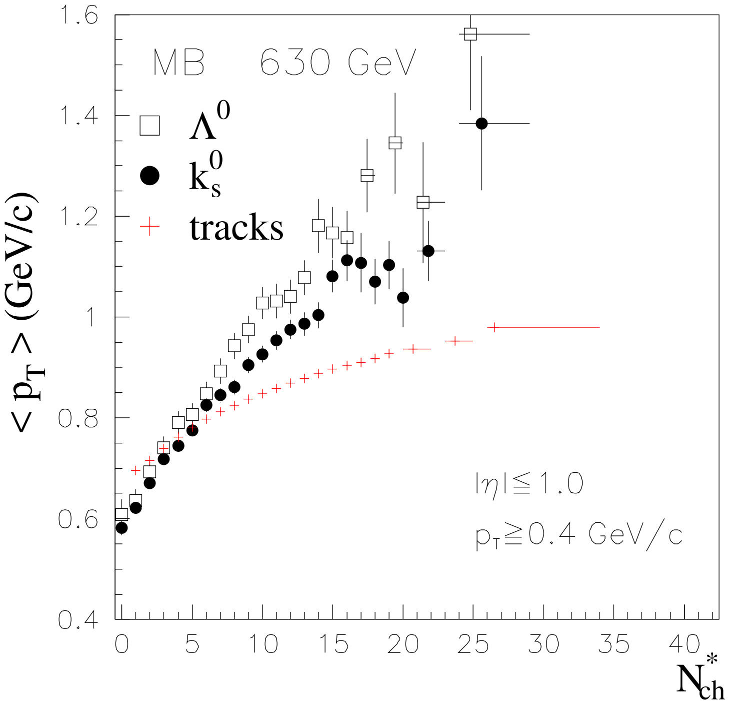

Figure 13: Average transverse momentum $\langle p_T \rangle$ of K_s^0 and Λ^0 at 630 GeV as a function of the event charged multiplicity ($N^{\star}_{ch}$). MB data are shown. For comparison, also the mean p_T of charged tracks, measured in the same phase space region, is plotted.

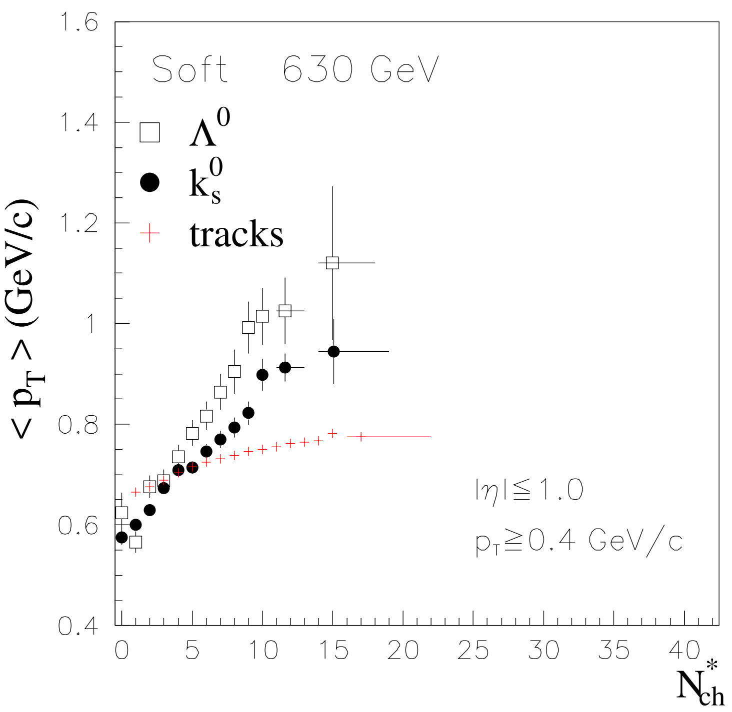

Figure 14: Average transverse momentum $\langle p_T \rangle$ of K_s^0 and Λ^0 at 630 GeV as a function of the event charged multiplicity ($N_{ch}^{\star}$). Soft data are shown. For comparison, also the mean p_T of charged tracks, measured in the same phase space region, is plotted.

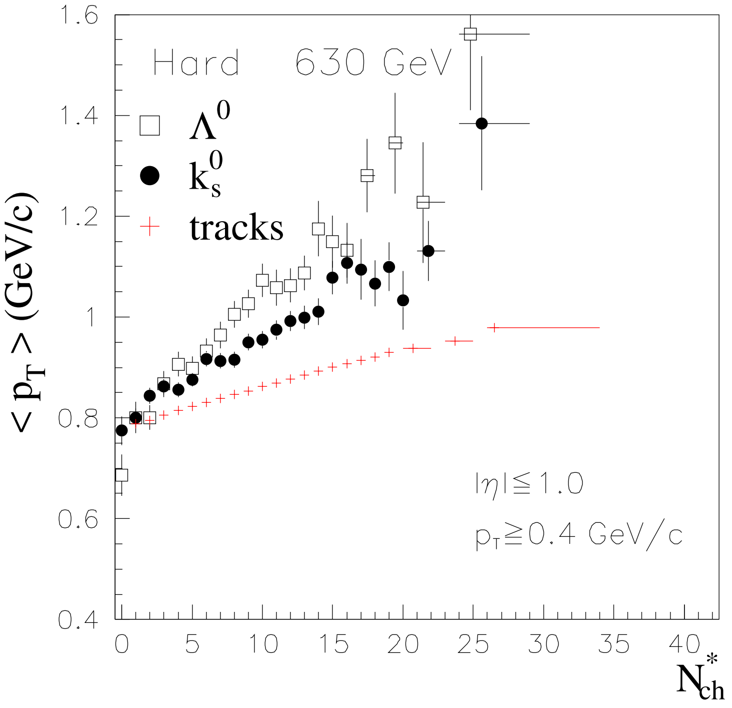

Figure 15: Average transverse momentum $\langle p_T \rangle$ of K_s^0 and Λ^0 at 630 GeV as a function of the event charged multiplicity ($N_{ch}^\star$). Hard data are shown. For comparison, also the mean p_T of charged tracks, measured in the same phase space region, is plotted.

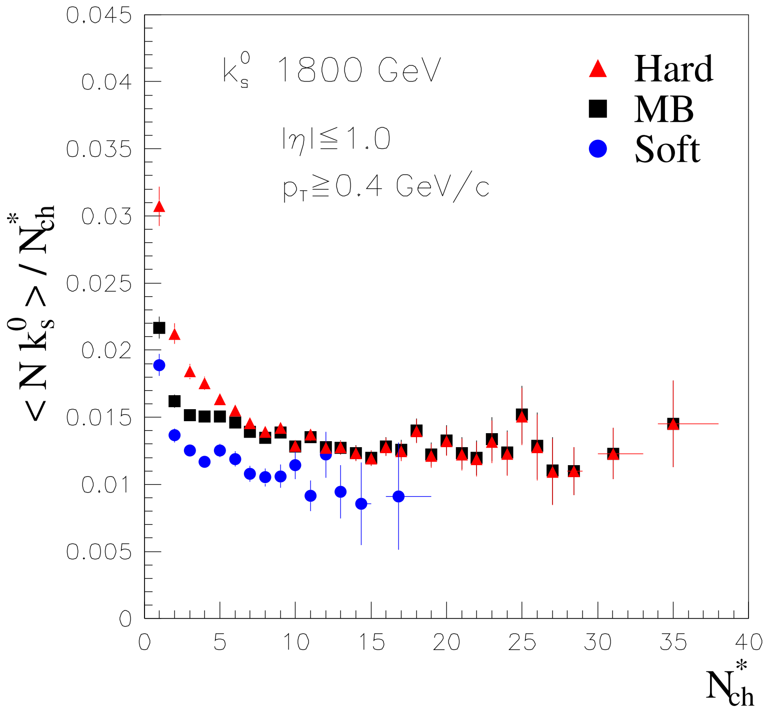

Figure 16: Mean number of K_s^0 per event divided by the charged multiplicity ($N^\star_{ch}$) and plotted as a function of $N^\star_{ch}$. The MB, soft and hard data at 1800 GeV are shown.

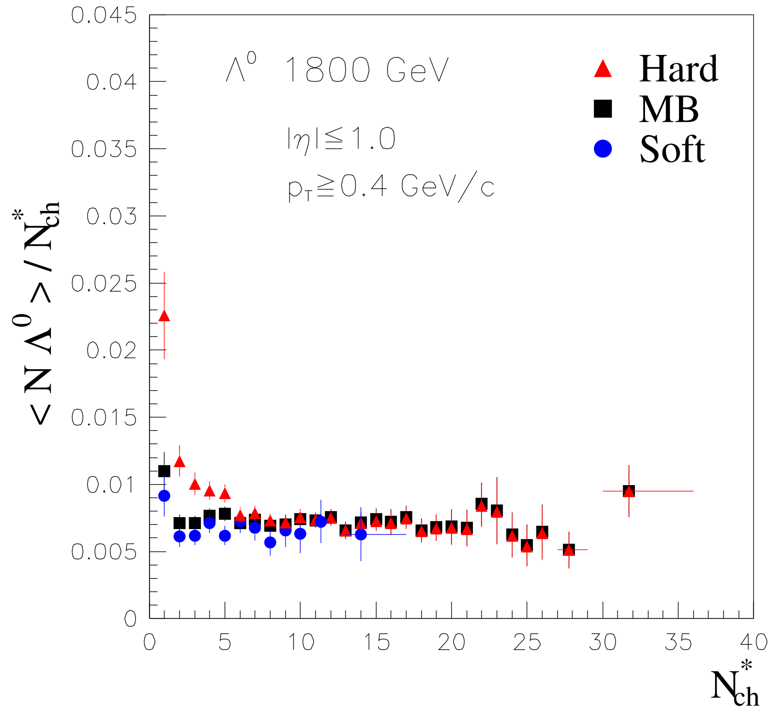

Figure 17: Mean number of K_s^0 per event divided by the charged multiplicity ($N_{ch}^{\star}$) and plotted as a function of $N_{ch}^{\star}$. The MB, soft and hard data at 630 GeV are shown.

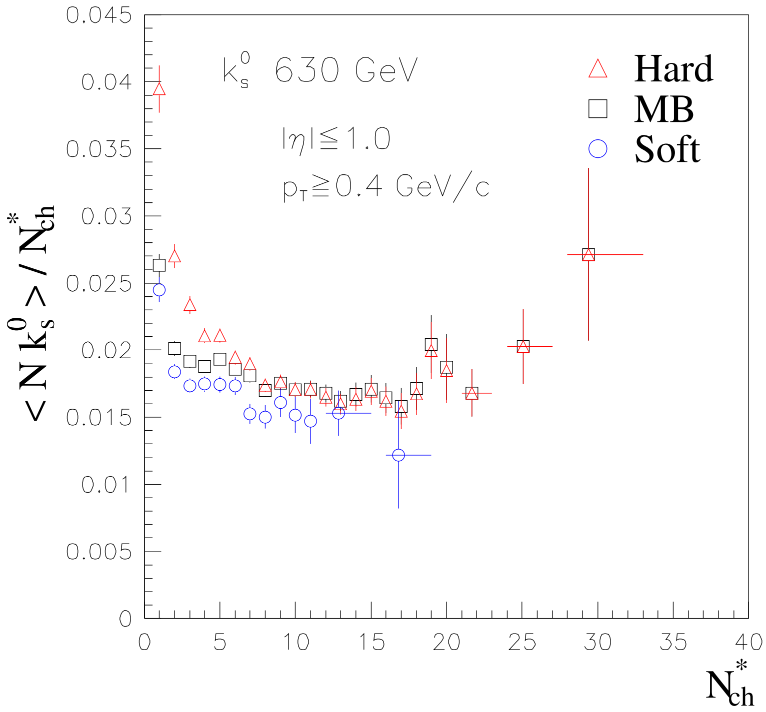

Figure 18: Mean number of Λ^0 per event divided by the charged multiplicity ($N_{ch}^\star$) and plotted as a function of $N_{ch}^\star$. The MB, soft and hard data at 630 GeV are shown.

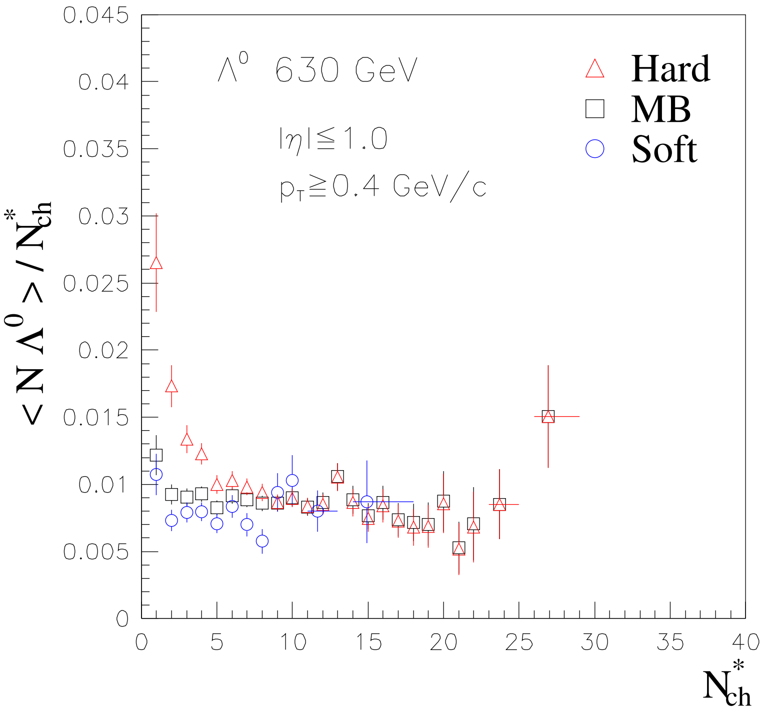

Figure 19: Mean number of Λ^0 per event divided by the charged multiplicity ($N^\star_{ch}$) and plotted as a function of $N^\star_{ch}$. The MB, soft and hard data at 630 GeV are shown.